Original Article

Development of a Fast Fourier Transform-based Analytical Method for COVID-19 Diagnosis from Chest X-Ray Images Using GNU Octave

Durjoy Majumder
Department of Physiology, West Bengal State University, Kolkata, West Bengal, India

Abstract

Purpose: Many artificial intelligence-based computational procedures are developed to diagnose COVID-19 infection from chest X-ray (CXR) images, as diagnosis by CXR imaging is less time consuming and economically cheap compared to other detection procedures. Due to unavailability of skilled computer professionals and high computer architectural resource, majority of the employed methods are difficult to implement in rural and poor economic settings. Majority of such reports are devoid of codes and ignores related diseases (pneumonia). The absence of codes makes limitation in applying them widely. Hence, validation testing followed by evidence-based medical practice is difficult. The present work was aimed to develop a simple method that requires a less computational expertise and minimal level of computer resource, but with statistical inference. **Materials and Methods:** A Fast Fourier Transform-based (FFT) method was developed with GNU Octave, a free and open-source platform. This was employed to the images of CXR for further analysis. For statistical inference, two variables, i.e., the highest peak and number of peaks in the FFT distribution plot were considered. **Results:** The comparison of mean values among different groups (normal, COVID-19, viral, and bacterial pneumonia [BP]) showed statistical significance, especially when compared to normal, except between viral and BP groups. **Conclusion:** Parametric statistical inference from our result showed high level of significance ($P < 0.001$). This is comparable to the available artificial intelligence-based methods (where accuracy is about 94%). Developed method is easy, availability with codes, and requires a minimal level of computer resource and can be tested with a small sample size in different demography, and hence, be implemented in a poor socioeconomic setting.

Keywords: Chest X-ray image, COVID-19, Fourier analysis, image analysis, pneumonia

Received on: 01-04-2022 **Review completed on: 13-06-2022** **Accepted on: 20-07-2022** **Published on: 08-11-2022**

Introduction

Severe acute respiratory syndrome (SARS-CoV) was first identified in December 2019 in Wuhan, China, caused by a novel corona virus COVID-19.[1] The disease had the animal origin, but transmitted from human to human through direct and indirect contacts, aerosols, and droplets. Since the time, it had spread all over the world. On January 30, 2020, the WHO declared that the outbreak of SARS-CoV-2 was a Public Health Emergency of International Concern.[2] The COVID-19 infection has onsets similar to other pneumonias.[3]

Conventionally, COVID-19 is detected either by reverse transcription–polymerase chain reaction (RT-PCR) or by computer tomography (CT) scan. At present, RT-PCR method has lower sensitivity (83.3%) compared to CT scan (97.2%).[4] Detection through RT-PCR takes several hours; but realistically, it takes several days due to samples are generally processed in bulk. Contrarily, CT scan machines are costly and hence may not be available in remote and rural areas. However, a chest X-ray-based (CXR) imaging method is less costly, generally available in remote and rural areas. Portable CXR machines are also available that enhances the feasibility in rural and even in hospital ward. Hence, due to continuation of the pandemic, a quick and cost-effective detection method of COVID-19 is indeed needed to stop further spread of the disease by isolating

Address for correspondence: Dr. Durjoy Majumder, Department of Physiology, West Bengal State University, Barasat, North 24 Parganas, Kolkata - 700 126, West Bengal, India.
E-mail: durjoy@rocketmail.com

Access this article online

Quick Response Code:

Website: www.jmp.org.in

DOI: 10.4103/jmp.jmp_26_22

This is an open access journal, and articles are distributed under the terms of the Creative Commons Attribution-NonCommercial-ShareAlike 4.0 License, which allows others to remix, tweak, and build upon the work non-commercially, as long as appropriate credit is given and the new creations are licensed under the identical terms.

For reprints contact: WKHLRPMedknow_reprints@wolterskluwer.com

How to cite this article: Majumder D. Development of a fast fourier transform-based analytical method for COVID-19 diagnosis from chest X-ray images using GNU octave. J Med Phys 2022;47:279-86.

the infected person. This may prevent community transmission. Moreover, an early detection can help to start the treatment early.[5-8] However, inferring of COVID-19 infection through CXR or CT scan requires an expert medical personnel, and in rural set-up, this may be unavailable. Moreover, due to sudden and massive increase of the pandemic situation, workload of medical personnel has increased tremendously. Hence, computational-based diagnosis will be an aid to the present situation.

In recent time, many attempts have made for the development of COVID-19 diagnosis through computational methods from CXR images and most of the methods followed AI (artificial intelligence) and deep learning-based algorithm [Table 1]. Although it is claimed that deep learning-based AI techniques can be used to ensure that the diagnosis is accurate, and so far through AI-based methods, 86% efficiency was achieved in diagnosing COVID-19 infection.[12,13,19] It is opined that machine learning algorithm requires a large and balanced datasets.[18] COVID-19 has many variants and different clinical manifestations in different individuals. A study with lung CT images showed that 60% of patients had bilateral lung infection, and 10.7% of patients had only right lung involvement and 5.7% of patients had only left lung involvement.[20,21] Image-based computational diagnostic methods rely on image pixels across the different anatomical localization of lungs. Hence, detection of COVID-19 infection for a clinical case from CXR images by matching with the large training dataset may not able to diagnose a particular case precisely. Changes in training dataset also change the accuracy level for COVID-19 detection from CXR images.[22] Moreover, AI-based methods are still not included in the evidence-based clinical practices.[23] Such limitations may restrict the use of AI-based method in a small demographic region. In majority of the cases, for COVID-19 detection from X-ray images by computational methods, codes are not available. Hence, to run those algorithms, more sophisticated computational resource, large dataset, and/or computational expertise are required.[19] These are also not available in rural set-up. Hence, a user-friendly algorithm and easily available framework are also needed. Moreover, majority of the AI-based algorithm for COVID-19 diagnosis are questionable due to different flaws including validation, code availability, consideration

Table 1: Comparison between different algorithms for detection of COVID-19

Model	Computer architecture and platform	Related diseases (sample size)	C19 cases (sample size)	Accuracy (%)	Specificity (%)	Reference
COVIDX-Net	Python and the Keras package with TensorFlow2 on Intel (R) Core (TM) i7-2.2 GHz processor	Nil	25	90	NA	Hemdan *et al*., 2020[9]
Convoluted CCN	NA	Pneumonia (500)	500	91.3 (C19), 88 (Pneumonia)	NA	Echtioui *et al*., 2020[10]
COVIDNet	MAC OS	Pneumonia (5538)	266	93.3	NA	Wang *et al*., 2020[8]
VGG-19	NA	Bacterial pneumonia (400), viral pneumonia (314)	224	93.48	98.75	Apostolopoulos and Mpesiana, 2020[11]
SSD	NA	Pneumonia* (647)	204	94.92	92	Saiz and Barandiaran, 2020[12]
DeTraC-ResNet18	MatLab 2019a in 3.70 GHz Intel (R) Core (TM) i3-6100 Duo, NVIDIA Corporation with the donation of the Quadra P5000GPU, and 8.00 GB RAM	SARS (11)	105	95.12	91.87	Abbas *et al*., 2020[13]
ResNet50+ SVM	MatLab 2019a in Acer Predator Helios 300 Core i5 8th Gen - (8 GB/1 TB HDD/128 GB SSD/Windows 10 Home/4 GB Graphics)	Bacterial pneumonia (63), viral pneumonia (64)	48	95.38	93.47	Sethy *et al*., 2020[14]
Heat Map CNN	NA	NA	NA	97.8	98	Kusakunniran *et al*., 2020[15]
Mask R-CNN	Python programming language in Windows environment using NVIDIA GTX 1080 4 GB GPU on a system with 8 GB RAM and having Intel Core-i5 7th generation @2.20GHz processor	Nil	534	96.98	97.36	Podder *et al*., 2021[16]
CNN	MATLAB 2020b online servers with 64-bit, 8-core, and 32 GB RAM	Pneumonia (NA) and tuberculosis (NA)	NA	98.55 (with 22 cases)	NA	Kaur *et al*., 2021[17]
Shallow CNN	NA	Viral and bacterial pneumonia is mixed to make balanced dataset (321)	321	99.32 (with a batch size of 25 cases)	99.09 (with a batch size of 25 cases)	Mukherjee *et al*., 2021[18]

*No mention of viral or bacterial pneumonia. NA: Not available, C19: COVID-19

of demography, and related diseases (bacterial and viral pneumonia [VP]).[24] Here, we have developed an algorithm within a free and open-source platform (software) and made simple statistical inference to distinguish between COVID-19, viral pneumonia (VP), and bacterial pneumonia (BP) cases.

The Fourier Transform is an important mathematical operational method used since 1965.[25] Application of this method in digital image processing was introduced with the development of Fast Fourier Transform (FFT) algorithm in 1970.[26] Through this method, an image is decomposed into its sine and cosine components. The output of the transformation represents the image in the Fourier or frequency domain, while the input image is the spatial domain equivalent. In the frequency domain of the image, each point represents a particular frequency contained in the spatial domain image. It is used in image processing for compression, restoration, resampling, edge detection and noise filtering, frequency, and time shift.[27,28] In the field of medicine, FFT has many applications for image processing and analysis, namely, reconstruction of discretized images of (CT) and (magnetic resonance imaging), ultrasound, and EEG signal analysis.[29-33]

Materials and Methods

Image datasets

The entire image dataset utilized in this study was collected from GitHub repository (https://github. com/arpanmangal/CovidAID). Randomly selected images of CXR (anterior–posterior) supine position of 200 normal (N), 200 COVID-19 infected (C19), 200 VP, and 200 BP were utilized in this study. GitHub has a library of publicly available collection of data that can be used further.[34-36] A representative samples of downloaded lung CXR images are shown in Figure 1.

Computational platform

All computer codes are developed in Octave platform. Octave is an open-source computational platform available freely from GNU Octave webpage (link url: https://www. gnu. org/software/octave/index). From the download page, Octave is downloaded with windows installer (link url: octave-6.2.0-w64-installer. exe) and installed from the installer in a Acer Aspire 1736Z Pentium ® Dual Core T4200 ® 2.00 GHz 6 GB RAM machine (with Windows 10 × 64) following the wizard. Octave is installed with default installation settings. Now, it is launched from the Start menu. The Octave version 6.2.0 has all the packages and installed by default settings and checked by "pkg list" command. However, if needed, io, control, signal, and image package are installed by execution of the following commands sequentially from the command window:

==========

Installation of Packages in Octave

==========

> pkg list

> pkg install -forge io

> pkg install -forge control

> pkg install -forge signal

> pkg install image-1.0.0.tar.gz

> pkg list

> pkg load io

> pkg load control

> pkg load signal

> pkg load image-1.0.0.tar.gz

==========

Installation and loading of packages are ensured with the "pkg list" command (it displays the list of all the installed packages with * marked).

2.3. Fourier Transform

The Fourier transform is also called a generalization of the Fourier series. This term can also be applied to both the frequency domain representation and the mathematical function used. The Fourier transform helps in extending the Fourier series to nonperiodic functions, which allows viewing any function as a sum of simple sinusoids.

The Fourier transform of a function *f(x)* is given by,

$$f(x) = \int_{-\infty}^{\infty} F(k) e^{2\pi i k x} dk$$

and the inverse Fourier transform is

$$f(x) = \int_{-\infty}^{\infty} F(k) e^{-2\pi i k x} dk$$

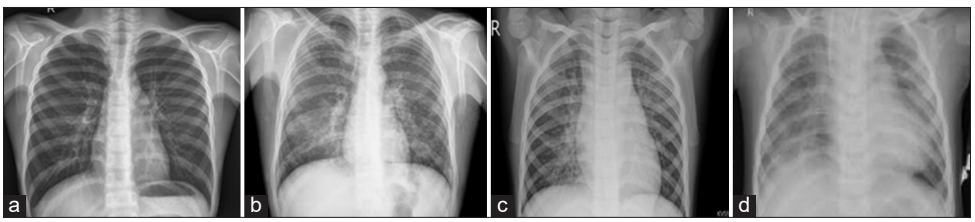

Figure 1: A representative sample of downloaded lung chest X-ray images from Github repository: Healthy asymptomatic normal (in a), diagnosed COVID-19 infected (in b), diagnosed viral pneumonia (in c), and diagnosed bacterial pneumonia (in d)

where *F(k)* can be obtained using inverse Fourier transform.

[*F (u, v)*] is the frequency domain representation of an image [*f (x, y)*] of size (*M* × *N*). Thus, 2D discrete Fourier transform is:

$$F(u,v)=\sum_{x=0}^{M-1}\sum_{y=0}^{N-1}f(x,y)e^{-i2\pi\left(\frac{ux}{M}+\frac{vy}{N}\right)}$$

Fourier transform concept is that any waveform can be constructed using a sum of sine and cosine waves of different frequencies. The exponential in the above formula expression can be expanded into sines and cosines with the variables u and v determining these frequencies. The inverse of the above discrete Fourier transform may be expressed as,

$$F(u,v)=\sum_{x=0}^{M-1}\sum_{y=0}^{N-1}f(x,y)e^{i2\pi\left(\frac{ux}{M}+\frac{vy}{N}\right)}$$

2.4. Algorithm of Fast Fourier Transform

FFT is performed through following algorithm.

Step 1: Open the original image through Paint and single lung (left or right) is cropped and save it with a different file name [Figure 2].

Step 2: Cropped image is read.

Step 3: Cropped image is converted to grayscale image.

Step 4: Now, the FFT shift technique is applied on grayscale image. FFT2 command computes the Discrete Fourier Transform of time series, and thus frequency domain signal is obtained from image. FFTSHIFT command moves the zero frequency component to the center of the spectrum. For vectors, FFTSHIFT (X) swaps the left and right half of X. For image matrices, FFTSHIFT (X) swaps the first and third quadrants, the second and fourth quadrants. Then, FFT shift in log scale is plotted. This makes the highest frequency at the center.

Step 5: From log FFT shift, a distribution plot is displayed to depict the frequency or pixels.

Step 6: Distribution plot is saved.

For FFT shift distribution, following codes are written in Editor Window and saved.

```
==========================================
Octave Code for FFT Shift & Distribution Plot
==========================================
close all
clear all
clc
#-- convert original image to grayscale image --------
img_gray = imread('C003R.bmp');
#grayscale_image=rgb2gray(img_gray);
figure(1);imshow(img_gray);
title('original image')
#figure(2); imshow(grayscale_image);
title('Grascale image')
print -djpg gray-image.bmp       # saving of grayscale image
#--convert grayscale image to log FFT shift image------
c = imread('gray-image.bmp');
cf = fftshift(fft2(c));
cr = radon(c);
figure(3);imshow(log(cf),[])
title('log FFT plot')
#print -djpg log-FFTshift.bmp    # to save log FFTshift image
#-- distribution plot (row vs column) from log FFT shift -----
c30 = fftshift(fft2(cr(:,180)));
c30l = log(1+abs(c30));
figure(4);plot(c30l)
title('distribution plot')
#print -djpg distribution.bmp   # saving of distribution image
==========================================
```

Before execution of the codes, file name of the image file is changed (also extension if needed). With the execution

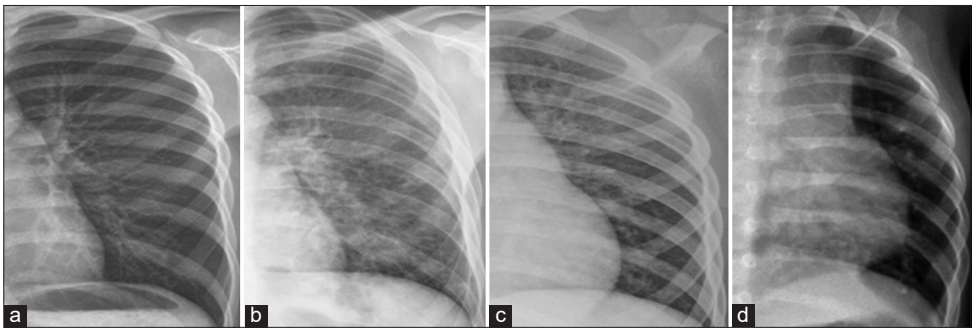

Figure 2: Left lung cropped images: healthy asymptomatic normal (in a), diagnosed COVID-19 infected (in b), diagnosed viral pneumonia (in c), and diagnosed bacterial pneumonia (in d)

from Run prompt, finally a distribution plot is generated. From the distribution plot, the highest peak value is noted and the number of peaks on both sides of the highest peak value is counted above a threshold value 12 (along the Y-axis) and such data are tabulated for both lungs. Threshold value is selected arbitrarily. Thus, the dataset has four columns and 800 rows, where each column have different variables (number of peaks of left lung, highest peak value of left lung, number of peaks of right lung, and highest peak value of right lung) and each row represents different CXR of normal, COVID-19, VP, and BP. For each CXR image, data of the highest peak values from both the lungs are averaged and tabulated in the fifth column.

Statistical analysis

Two-sided *t*-test is performed for significance of analysis between the mean values of different groups in pair (the groups are C19 and N, VP and N, VP and C19, BP and N, BP and C19, and BP and VP). Further, in an understanding of data variability of each samples in different disease (infected) groups (C19, VP, and BP), we have performed principal component analysis (PCA) and linear discriminant analysis (LDA).

Results

With the selection of image file name, the FFT code is executed from run tab; then, the whole code runs automatically. Image file is read and displayed, followed by saving of the image (with gray conversion, if any color is present) and plot of FFT shift, and distribution plot is displayed [Figures 3 and 4].

From distribution plot, data (highest peak value and number of peaks above a threshold value, as mentioned in the previous section) are collected. From each of the CXR image, data are tabulated. Statistical measures and inference between different groups (C19 and N, VP and N, VP and C19, BP and N, BP and C19, and BP and VP) are evaluated by the *t*-test, and results are tabulated in Tables 2-4. In all the cases, $P < 0.001$ is considered statistically significant. Comparing the mean values of the highest peak value (from distribution plot of both left and right lungs) between groups (N vs. C19, N vs. VP, C19 vs. VP, C19 vs. BP, and BP vs. VP), it shows a statistical significant difference. Comparing the mean value for the number of peaks for left lung between groups (N vs. C19, N vs. VP, C19 vs. VP, N vs. BP, and C19 vs. BP), it shows a statistical significant difference. Comparing the mean value for the number of peaks for right lung between groups (N vs. C19, N vs. VP, C19 vs. VP, N vs. BP, and C19 vs. BP), it shows a statistical significant difference. Results indicate that the mean value of the maximum peak value of BP and normal (N) is almost similar. From the mean value of number of peaks, it is also difficult to distinguish between VP and BP groups for both the lungs. These results are not statistically significant (NS).

To understand the data, variability/clustering pattern is analyzed further in different infected groups (600 × 4, 200 samples for each group and two variables of two lungs) by PCA and LDA. In both the analyses, BP group is partially overlapped with VP groups; in LDA, it is more prominent than PCA-based clustering [Figure 5].

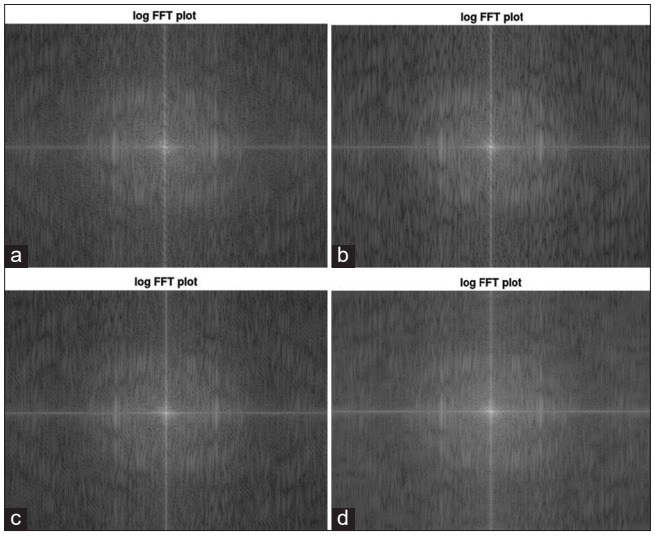

Figure 3: FFT shift of cropped images: Healthy asymptomatic normal (in a), diagnosed COVID-19 infected (in b), diagnosed viral pneumonia (in c), and diagnosed bacterial pneumonia (in d). FFT: Fast Fourier Transform

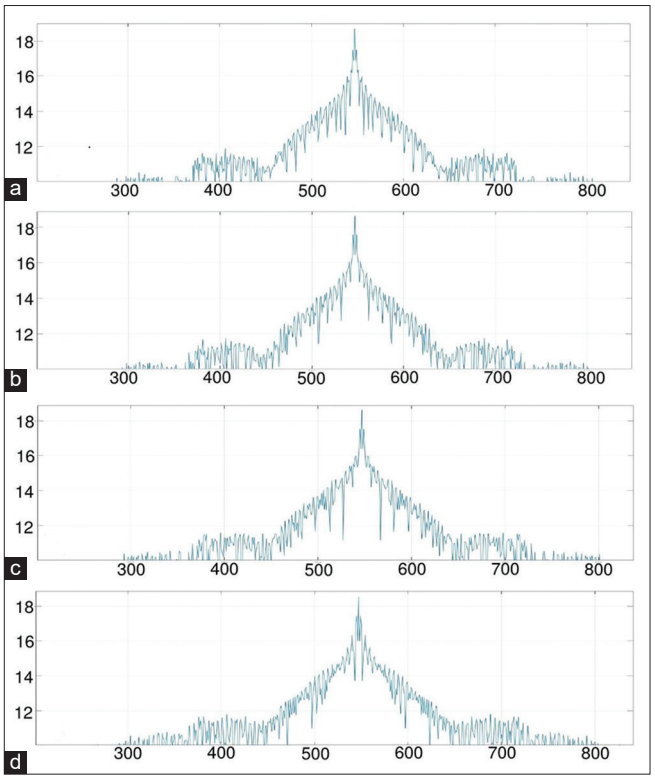

Figure 4: FFT distribution plot of each cropped lung image: Healthy asymptomatic normal (in a), diagnosed COVID-19 infected (in b), diagnosed viral pneumonia (in c), and diagnosed bacterial pneumonia (in d). The highest peak value is noted and the number of peaks on both sides of the highest peak value is counted above a threshold value 12 (along the Y-axis). FFT: Fast Fourier Transform

Table 2: The statistical measures of inference for average value (left and right lung) of maximum peak value (along Y-axis) obtained from distribution plot of chest X-ray images between different groups

Variable	N	C19	VP	BP
Sample size	200	200	200	200
Maximum	18.7020	18.720	18.6910	18.6950
Minimum	18.2735	18.600	18.5275	18.4580
Mean	18.5930	18.664	18.6390	18.5810
Median	18.6185	18.660	18.6480	18.5790
SD	0.081	0.0305	0.036	0.048
P		6.19061E-27 (N)	4.418E-13 (N) 3.404E-14 (C19)	0.067867 (N) (NS) 2.810E-63 (C19) 1.422E-35 (VP)

P value is obtained in comparison between different groups (compared group is mentioned in parentheses), if the obtained $P \geq 0.05$, it is considered statistically NS. SD: Standard deviation, VP: Viral pneumonia, BP: Bacterial pneumonia, C19: COVID-19, N: Normal, NS: Not significant

Table 3: The statistical measures of inference from number of peaks in the left lung obtained from distribution plot of chest X-ray images between different groups

Variable	N	C19	VP	VP
Sample size	200	200	200	200
Maximum	52	44	60	60
Minimum	28	32	34	36
Mean	32.51	37.75	49.32	49.065
Median	32	36	52	49.5
SD	3.693	3.987	6.326	6.779
P		4.59438E-37 (N)	1.496E-113 (N) 3.896E-65 (C19)	4.48726E-98 (N) 5.40E-52 (C19) 0.069 (VP) (NS)

P value is obtained in comparison between different groups (compared group is mentioned in parentheses), if the obtained $P \geq 0.05$, it is considered statistically NS. SD: Standard deviation, VP: Viral pneumonia, BP: Bacterial pneumonia, C19: COVID-19, N: Normal, NS: Not significant

Table 4: The statistical measures of inference from number of peaks in the right lung obtained from distribution plot of chest X-ray images between different groups

Variable	N	C19	VP	BP
Sample size	200	200	200	200
Maximum	42	44	58	58
Minimum	28	32	36	34
Mean	32.06	38.37	49.2	50.18
Median	32	38	50	52
SD	2.898	3.985	5.111	6.889
P		7.80829E-54 (N)	1.7482E-145 (N) 3.932E-76 (C19)	7.9476E-121 (N) 1.707E-62 (C19) 0.101 (VP) (NS)

Our data clearly suggest that FFT-based algorithm can clearly distinguish between normal and COVID-19 infection as well as between pneumonia (viral or bacterial) and COVID-19 infection (mean values between the groups are statistically significant); but unable to differentiate between viral and BP. The data of distribution plot analysis indicate that in pneumonia cases, spread of infection within lung is more compared to COVID-19 infection cases. Therefore, it can be apprehended that COVID-19 infection is clustered to some regions of lungs. It is to be noted here that the maximum peak value of the distribution plot is in the following order:

Normal > COVID-19 > Viral pneumonia≅ Bacterial pneumonia; in BP, even height of the highest peak value is almost same compared to normal.

Discussion

For easy feasibility, cheap and fast approach of CXR, several methods for COVID-19 detection through computational approach are developed for COVID-19 detection in the past 2 years. Most of the methods are based on deep learning and AI-based. With this approach so far, the maximum accuracy level has reached 98.55%; however, those reports have several disadvantages– sample size for accuracy testing either missing or very limited and many methods do not compare related symptomatic problems like pneumonia,[3] and if considered, they have coupled viral and BP in accuracy testing [Table 1]. Considering such similar types of infections, about 86% is the maximum accuracy level reached.[19] Moreover, in majority of the published works on methodologies, codes are either not available or available in nonstandardized public domain. Although in this field many computer scientists are working and many consider it as manual-like representation, the unavailability of codes limits its further use and hence clinical applications.[24,37] Moreover, it is an undeniable fact, employing of deep learning- and AI-based methods requires more sophisticated computational resource and computer-trained personnel, both are difficult to get in rural and poor socioeconomic setting. There is also a lack of necessary mandate of using AI in clinical application to seek evidence-based medical practices, especially in the era of 4IR.[23] Although in recent time, vaccination initiative has started, several persons are still getting infected even after receiving vaccine. Hence, to start treatment early and to prevent community transmission further, still there is a demand of cheap and easier diagnostic procedure of COVID-19 infection. Here, the main purpose of the work is to develop a computational method that is easy to handle with minimal level of computational resource and expertise. Hence, detail procedures are available in step-wise manner.

Here, the developed algorithm is numerical- and statistics-based, considers only two variables (highest peak value and number of peaks); hence, easy to implement in rural and poor socioeconomic condition. Moreover, in majority of the

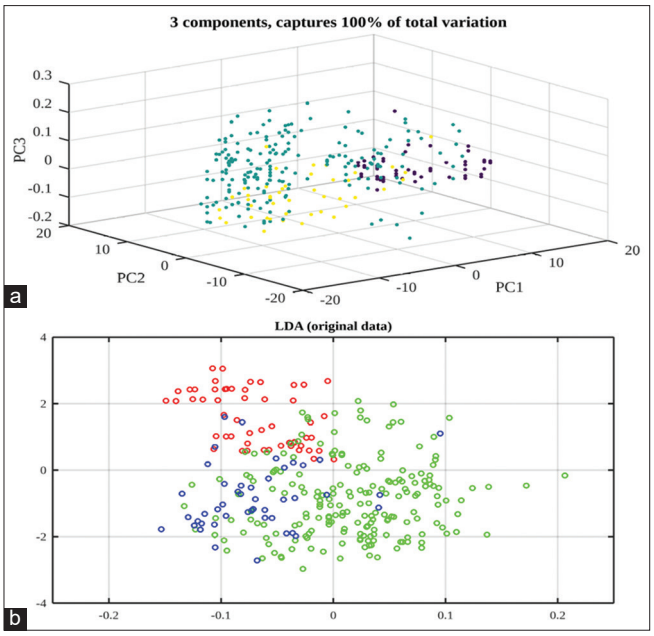

Figure 5: Clustering of data in different infected groups by PCA (in a) and LDA (in b). PCA: Principal component analysis, LDA: Linear discriminant analysis

published methods on COVID-19 detection from the chest images, algorithmic codes are not available. Here, to address the issues as in reference,[24] we have elaborated all the steps and codes. For number of peak counts, the threshold value 12 is selected arbitrarily, and this is considered in the assessment for all the samples. Other workers can select other value, but should maintain the same value for the assessment of all other samples.

With a large dataset having 20 hospitals across the globe, deep transfer learning-based method differentiates COVID-19 and COVID-19-induced pneumonia with 94% accuracy.[38] However, in another work, it is reported that changing of dataset ANN-based method showed differences in accuracy in detection (94% and 85%), and it also requires large dataset for training purpose.[22] Hence, if images are collected from a single demography and with the same machine, then comparing the mean values between normal volunteers and individual patients' data will help detect COVID-19 infection in individual patient. With this method, COVID-19 infection is differentiated from pneumonia (bacterial and viral); however, with this method, differentiation between bacterial and VP cannot be differentiated. It is needless to mention here that so far no AI- and deep learning-based machine learning algorithm can differentiate between the two. We have made analysis with the images available in public domain, and the images are captured with different machines and possibly from different demographics; however, statistical inference is highly significant ($P < 0.001$), the calculated P value in turn shows high level of accuracy and sensitivity compared to existing AI-based methods.

This method utilizes FFT-based analysis of pixels distribution (distribution plot); hence, another important finding of the work is that COVID-19 infection may be clustered to some regions of lungs; while in pneumonia cases, infection spreading within lung is more. We could not find any significant difference between the left and right lung data within the same group, this in turn, may indicate that there is no specificity of infection among lungs, especially with COVID-19 infection. A work utilizes texture, GLDM, GLCM, FFT, and wavelet for feature extractions, followed by uses machine learning classifier to classify normal, COVID-19, and pneumonia with 94% accuracy.[37] This work utilizes FFT-based data of two variables which make an ease to perform an elementary parametric-based statistical analysis; hence, contrary to AI-based methods, it does not require large datasets; however, contribute more substantially to evidence-based diagnosis.[39] Such statistical operations are very elementary and available under statistical menu of the spreadsheet program in Office software, both in Microsoft and LibreOffice (another free and open-source software). The developed code is in Octave, a free open-source platform, and it can be installed to a computer with minimum configuration; runtime of the code is a few seconds, and hence, computational cost is very low. All these advantages make the method simple.

Conclusion

The developed method is based on simple codes (which are also available here) in Octave platform and requires a minimal computer resource, so this can be employed in poor and low socioeconomic setting. It can be accepted and implemented universally to include in different and even in small demography without waiting for large data for generating training dataset as in AI. A suspected patient's CXR image is collected and made a FFT-based analysis. Numerical values obtained from the distribution plot of FFT analysis (number of peaks) will be compared to the mean ± standard deviation value of normal; then, a follow-up to be made by isolating the patients and if possible, can be referred for further investigation. Although the mean value of the highest peak showed statistical significance among groups, the differences are very less; hence, monitoring the value in the number of peaks is important and can practically be possible. We hope that this analytical method could be applied immediately to combat the community spread of COVID-19 infection and to stop this pandemic situation and ultimately causes eradication of the disease.

Acknowledgment

The author acknowledges the critical comments and suggestions of Dr. Dibyendu Kumar Ray, Senior Consultant of Neurosurgery, AMRI Hospital and President, Society for Systems Biology and Translational Research about this work.

Financial support and sponsorship

Nil.

Conflicts of interest

There are no conflicts of interest.

References

1. Zhu N, Zhang D, Wang W, Li X, Yang B, Song J, *et al.* A novel coronavirus from patients with pneumonia in China, 2019. N Engl J Med 2020;382:727-33.
2. Xu G, Yang Y, Du Y, Peng F, Hu P, Wang R, *et al.* Clinical pathway for early diagnosis of COVID-19: Updates from experience to evidence-based practice. Clin Rev Allergy Immunol 2020;59:89-100.
3. Zhao D, Yao F, Wang L, Zheng L, Gao Y, Ye J, *et al.* A comparative study on the clinical features of coronavirus 2019 (COVID-19) pneumonia with other pneumonias. Clin Infect Dis 2020;71:756-61.
4. Long C, Xu H, Shen Q, Zhang X, Fan B, Wang C, *et al.* Diagnosis of the coronavirus disease (COVID-19): rRT-PCR or CT? Eur J Radiol 2020;126:108961.
5. Toussie D, Voutsinas N, Finkelstein M, Cedillo MA, Manna S, Maron SZ, *et al.* Clinical and chest radiography features determine patient outcomes in young and middle-aged adults with COVID-19. Radiology 2020;297:E197-206.
6. Cellina M, Gibelli D, Valenti Pittino C, Toluian T, Marino P, Oliva G. Risk factors of fatal outcome in patients with COVID-19 pneumonia. Disaster Med Public Health Prep 2022;16:271-8.
7. Cellina M, Panzeri M, Oliva G. Chest radiography features help to predict a favorable outcome in patients with coronavirus disease 2019. Radiology 2020;297:E238.
8. Wang L, Lin ZQ, Wong A. COVID-Net: A tailored deep convolutional neural network design for detection of COVID-19 cases from chest X-ray images. Sci Rep 2020;10:19549.
9. Hemdan EE, Shouman MA, Karar ME. Covidx-net: A framework of deep learning classifiers to diagnose covid-19 in x-ray images. ArXiv 2020. Available from : https://arxiv.org/abs/2003.11055. [Last accessed on 2022 Jan 03].
10. Echtioui A, Zouch W, Ghorbel M, Mhiri C, Hamam H. Detection methods of COVID-19. SLAS Technol 2020;25:566-72.
11. Apostolopoulos ID, Mpesiana TA. Covid-19: Automatic detection from X-ray images utilizing transfer learning with convolutional neural networks. Phys Eng Sci Med 2020;43:635-40.
12. Saiz FA, Barandiaran I. COVID-19 detection in chest X-ray images using a deep learning approach. Int J Interact Multim Artif Intell 2020;6:1-4.
13. Abbas A, Abdelsamea MM, Gaber MM. Classification of COVID-19 in chest X-ray images using DeTraC deep convolutional neural network. Appl Intell (Dordr) 2021;51:854-64.
14. Sethy PK, Behera SK, Ratha PK, Biswas P. Detection of coronavirus disease (COVID-19) based on deep features and support vector machine. Int J Math Eng Mang Sci 2020;5:643-51.
15. Kusakunniran W, Karnjanapreechakorn S, Siriapisith T, Borwarnginn P, Sutassananon K, Tongdee T, *et al.* COVID-19 detection and heatmap generation in chest x-ray images. J Med Imaging (Bellingham) 2021;8:014001.
16. Podder S, Bhattacharjee S, Roy A. An efficient method of detection of COVID-19 using mask R-CNN on chest X-Ray images. AIMS Biophys 2021;8:281-90.
17. Kaur M, Kumar V, Yadav V, Singh D, Kumar N, Das NN. Metaheuristic-based deep COVID-19 screening model from chest X-ray images. J Healthc Eng 2021;2021:8829829.
18. Mukherjee H, Ghosh S, Dhar A, Obaidullah SM, Santosh KC, Roy K. Shallow convolutional neural network for COVID-19 outbreak screening using chest X-rays. Cognit Comput 2021; Data-Driven Artificial Intelligence approaches to Combat Covid-19:1-14. doi: https://doi.org/10.1007/s12559-020-09775-9.
19. Bhattacharya S, Reddy Maddikunta PK, Pham QV, Gadekallu TR, Krishnan SS, Chowdhary CL, *et al.* Deep learning and medical image processing for coronavirus (COVID-19) pandemic: A survey. Sustain Cities Soc 2021;65:102589.
20. Ozma MA, Maroufi P, Khodadadi E, Köse Ş, Esposito I, Ganbarov K, *et al.* Clinical manifestation, diagnosis, prevention and control of SARS-CoV-2 (COVID-19) during the outbreak period. Infez Med 2020;28:153-65.
21. Bernheim A, Mei X, Huang M, Yang Y, Fayad ZA, Zhang N, *et al.* Chest CT findings in coronavirus disease-19 (COVID-19): Relationship to duration of infection. Radiology 2020;295:200463.
22. Manav M, Goyal M, Kumar A, Arya AK, Singh H, Yadav AK. Deep learning approach for analyzing the COVID-19 chest X-rays. J Med Phys 2021;46:189-96.
23. Otokiti AU. Digital health and healthcare quality: A primer on the evolving 4th industrial revolution. In: Stawicki SP, Firstenberg MS, editors. Contemporary Topics in Patient Safety. London: IntechOpen; 2022. p. 1-20.
24. Roberts M, Driggs D, Thorpe M, Gilbey J, Yeung M, Ursprung S, *et al*. Common pitfalls and recommendations for using machine learning to detect and prognosticate for COVID-19 using chest radiographs and CT scans. Nat Mach Intell 2021;3:199-217. Available from: https://doi.org/10.1038/s42256-021-00307-0.
25. Cooley JW, Tukey JW. An algorithm for the machine calculation of complex Fourier series. Math Comput 1965;19:297-301.
26. Harmuth HF. Transmission of Information by Orthogonal Functions. Berlin, Germany: Springer; 1970.
27. Smith SW. Linear image processing. In: The Scientist and Engineer's Guide to Digital Signal Processing. Ch. 24. San Diego: California Technical Publishing; 1997. p. 397-422.
28. Yaroslavsky LP. Fast transforms in image processing: Compression, restoration, and resampling. Adv Electr Eng 2014;2014:276241.
29. Yoshimasu T, Kawago M, Hirai Y, Ohashi T, Tanaka Y, Oura S, *et al.* Fast Fourier transform analysis of pulmonary nodules on computed tomography images from patients with lung cancer. Ann Thorac Cardiovasc Surg 2015;21:1-7.
30. Kim GY, Lee JH, Hwang YN, Kim SM. A novel intensity-based multi-level classification approach for coronary plaque characterization in intravascular ultrasound images. Biomed Eng Online 2018;17:151.
31. Prasad BV, Parthasarathy V. Detection and classification of cardiovascular abnormalities using FFT based multi-objective genetic algorithm. Biotechnol Biotechnol Equip 2018;32:183-93.
32. Pontone G, Weir-McCall JR, Baggiano A, Del Torto A, Fusini L, Guglielmo M, *et al.* Determinants of rejection rate for coronary CT angiography fractional flow reserve analysis. Radiology 2019;292:597-605.
33. van der Zande JJ, Gouw AA, van Steenoven I, van de Beek M, Scheltens P, Stam CJ, *et al.* Diagnostic and prognostic value of EEG in prodromal dementia with Lewy bodies. Neurology 2020;95:e662-70.
34. Cohen JP, Morrison P, Dao L. Covid-19 image data collection. ArXiv 2020. Available from: https://github.com/ieee8023/covid-chestxray-dataset. [Last accessed on 2022 Jan 03].
35. Mooney P, Kaggle Chest x-Ray Images (pneumonia) Dataset; 2018. Available from: https://www.kaggle.com/paultimothymooney/chest-xray-pneumonia. [Last accessed on 2022 Jan 03].
36. Kermany DS, Goldbaum M, Cai W, Valentim CC, Liang H, Baxter SL, *et al.* Identifying medical diagnoses and treatable diseases by image-based deep learning. Cell 2018;172:1122-31.e9.
37. Zargari Khuzani A, Heidari M, Shariati SA. COVID-Classifier: An automated machine learning model to assist in the diagnosis of COVID-19 infection in chest X-ray images. Sci Rep 2021;11:9887.
38. Brima Y, Atemkeng M, Tankio Djiokap S, Ebiele J, Tchakounté F. Transfer learning for the detection and diagnosis of types of pneumonia including pneumonia induced by COVID-19 from chest X-ray images. Diagnostics (Basel) 2021;11:1480.
39. Rubin A. Use of statistics in evidence based practice. In: Statistics for Evidence-Based Practice and Evaluation. 3rd ed. Canada: CENGAGE Learning; 2010. p. 11-20.